Hsa_circ_0050900 affects ferroptosis in intrahepatic cholangiocarcinoma cells by targeting hsa-miR-605-3p to regulate SLC3A2

XIANGTIAN SHI[1], JIARUI YANG[2,3], MENG WANG[1], LONG XIA[4], LEI ZHANG[3] and SHAN QIAO[1]

[1]Department of Hepatobiliary Surgery, Bayannur Hospital, Bayannur, Inner Mongolia Autonomous Region 015000; [2]Department of Hepatobiliary, Pancreatic and Splenic Surgery, Affiliated Dongguan Hospital, Southern Medical University (Dongguan People's Hospital), Dongguan, Guangdong 523058; [3]Department of Pancreatic Hepato-Biliary-Surgery, The Sixth Affiliated Hospital, Sun Yat-sen University, Guangzhou, Guangdong 510655; [4]Department of Hepatobiliary-Pancreatic-Splenic Surgery, Inner Mongolia Autonomous Region People's Hospital, Hohhot, Inner Mongolia Autonomous Region 010017, P.R. China

Received October 11, 2022; Accepted September 20, 2023

DOI: 10.3892/ol.2023.14135

Abstract. Intrahepatic cholangiocarcinoma (ICC) is a highly lethal hepatobiliary tumor with high aggressiveness. The role of circular RNA (circRNA) in ICC remains to be explored. The present study aimed to investigate whether hsa_circ_0050900 affected ferroptosis in ICC cells by regulating hsa-microRNA (miR)-605-3p/solute carrier family 3 member 2 (SLC3A2). Human ICC cells were cultured and hsa_circ_0050900 expression was evaluated by reverse transcription-quantitative PCR. hsa_circ_0050900 was knocked down and ferroptosis inhibitor ferrostatin-1 was added to HuCCT-1 cells. Following knockdown or overexpression of hsa-miR-605-3p, Fe^{2+}, reactive oxygen species (ROS), glutathione peroxidase 4 and SLC3A2 levels were assessed using iron and ROS assay kit or RT-qPCR and western blotting, respectively. Cell function experiments were performed to examine proliferation and migration abilities. Dual-luciferase reporter gene and argonaute2-RNA immunoprecipitation assay verified the relationship among hsa_circ_0050900, hsa-miR-605-3p, and SLC3A2. hsa_circ_0050900 was derived from actinin alpha 4 gene and was elevated in ICC cells. Among HuCCT-1, QBC-939, HCCC-9810, and RBE cell lines, the highest expression was in HuCCT-1 cells. Inhibition of hsa_circ_0050900 inhibited proliferation and migration by facilitating ICC cell ferroptosis. hsa-miR-605-3p expression was elevated after knocking down hsa_circ_0050900 and hsa-miR-605-3p was negatively regulated by hsa_circ_0050900. In addition, hsa-miR-605-3p targeted SLC3A2. Overexpression of hsa-miR-605-3p regulated SLC3A2 to promote ICC cell ferroptosis and inhibit proliferation and migration. Taken together, knockdown of hsa_circ_0050900 inhibited SLC3A2 expression via sponging hsa-miR-605-3p to promote ICC cell ferroptosis, and finally suppressed proliferation and migration. The present study suggested that hsa_circ_0050900 was a potential therapeutic target for ICC.

Correspondence to: Professor Shan Qiao, Department of Hepatobiliary Surgery, Bayannur Hospital, 98 Wulanbuhe Road, Bayannur, Inner Mongolia Autonomous Region 015000, P.R. China
E-mail: 3283518207@qq.com

Dr Lei Zhang, Department of Pancreatic-Hepato-Biliary-Surgery, The Sixth Affiliated Hospital, Sun Yat-sen University, 26 Erheng Road, Guangzhou, Guangdong 510655, P.R. China
E-mail: dw8316291@163.com

Abbreviations: ICC, intrahepatic cholangiocarcinoma; circ, circular; nc, non-coding; SLC3A2, solute carrier family 3 member 2; WT, wild-type; MUT, mutant; RT-q, reverse transcript-quantitative; ROS, reactive oxygen species

Key words: hsa_circ_0050900, hsa-microRNA-605-3p, SLC3A2, intrahepatic cholangiocarcinoma, ferroptosis, migration

Introduction

Intrahepatic cholangiocarcinoma (ICC) is a highly lethal hepatobiliary tumor with a 140% increasing incidence in worldwide over the past 4 decades (1-3). ICC is characterized by aggressive progression, connective tissue hyperplasia and vascular abnormalities (4). Complete surgical resection remains the only cure for patients with ICC but only one third of patients have resectable ICC (5). For patients with unresectable or metastatic disease, combine systemic and local therapies (such as radioembolization or hepatic artery infusion) and targeted therapies (such as target fibroblast growth factor receptor and isocitrate dehydrogenase) are required (3). Ferroptosis is an iron-dependent cell death pathway involved in a number of diseases, such as acute myeloid leukaemia, T-cell leukaemia/lymphoma, and COVID-19 infections (6). In recent years, ferroptosis has attracted a great deal of interest in cancer research, such as non-small-cell lung cancer, breast cancer, gastric cancer and liver cancer (7-9). Ferroptosis is considered to be a tumor suppressor and a novel target for

tumor therapy (6). However, the specific mechanism of ICC and ferroptosis remains unclear.

Circular RNAs (circRNAs) are non-coding RNAs containing covalently closed loops that are characterized by abundance, stability, conservation and tissue specificity (10). In cancer, circRNAs serve essential regulatory roles, including tumor-promoting and tumor-suppressing activity. Elevated circRNA cGGNBP2 (a circular RNA derived from exons 4-6 of the gametogenetin binding protein 2 gene) is associated with poor prognosis in patients with ICC and is an independent risk factor for prognosis (11). Furthermore, circRNA SWI/SNF related, matrix associated, actin dependent regulator of chromatin, subfamily a, member 5 is associated with favorable clinical tumor characteristics and prognosis and increased ICC chemosensitivity (12). A previous study reported that circRNA actinin alpha 4 (ACTN4), also named as hsa_circ_0050900, is highly expressed in breast cancer and competitively binds to the far upstream element binding protein 1 to prevent the combination of far upstream element binding protein 1 and FBP interacting repressor, thereby activating Myc transcription and facilitating tumor progression (13). Furthermore, circACTN4 (hsa_circ_0050898), another circRNA derived from ACTN4, is upregulated in ICC and promotes ICC cell proliferation and metastasis by regulating the target microRNA (miR)-424-5p, as well as transcriptional activation of Frizzled-7, by interacting with Y-box binding protein 1 (14). However, whether hsa_circ_0050900 is involved in ferroptosis in ICC is unknown.

hsa-miR-605-3p is reported to play a tumor suppressor role in different types of cancer: For example, miR-605-3p is downregulated in colon cancer and overexpression of miR-605-3p inactivates the Wnt/β-catenin signaling pathway induced by overexpression of kinesin family member 3B (15). In bladder cancer, overexpression of circRNA VANGL planar cell polarity protein 1 inhibits the availability of miR-605-3p to promote the expression of VANGL planar cell polarity protein 1, and the cancer cell proliferation, migration and invasion (16). Additionally, miR-605-3p is downregulated in glioma and high expression of miR-605-3p decreases the expression of target vasodilator stimulated phosphoprotein to inhibit glioma cell proliferation, migration and invasion (17). miR-605-3p is lowly expressed in hepatocellular carcinoma and small nucleolar RNA host gene 16/miR-605-3p/TNF receptor associated factor 6/NF-κB feedback loop participates in development of hepatocellular carcinoma (18). Moreover, miR-605 is lowly expressed in ICC and regulates ICC progression by controlling the downstream target gene proteasome 26S subunit, non-ATPase 10 (19). However, whether hsa_circ_0050900 regulates hsa-miR-605-3p to participate in ferroptosis in ICC cells is unknown.

Solute carrier family 3 member 2 (SLC3A2), also called CD98hc or 4F2hc, is a type II membrane protein (20,21). SLC3A2 and SLC7A11 are key targets for ferroptosis. The role of SLC7A11 in different types of cancer has been widely explored in recent years; to the best of our knowledge, however, there are few studies on SLC3A2 (22,23). SLC3A2 and its light chain subunit constitute a heterodimeric transmembrane complex that mediates amino acid transport and regulates mTOR and macroautophagy/autophagy (24). In lung adenocarcinoma, YTH N6-methyladenosine RNA binding protein C2 serves as an endogenous ferroptosis inducer and inhibits SLC3A2 expression (25). In addition, SLC3A2 negatively regulates ferroptosis in laryngeal carcinoma via the mTOR pathway (26). SLC3A2 inhibits ferroptosis and suppresses cartilage degeneration in osteoarthritis (27). Moreover, liver cancer cells with hepatitis B virus infection-derived exosomal miR-142-3p exhibit increased M1-type macrophage ferroptosis by inhibiting expression of target SLC3A2 (28). However, it is unknown whether hsa_circ_0050900 regulates SLC3A2 by sponging hsa-miR-605-3p and thus affecting ferroptosis in ICC.

The present study aimed to explore hsa_circ_0050900/hsa-miR-605-3p/SLC3A2 signaling in ICC cell ferroptosis and the molecular mechanism underlying ICC occurrence and development to facilitate development of novel therapeutic targets.

Materials and methods

Cell culture and treatment. Human ICC-derived QBC-939, HUCCT-1, HCCC-9810 and RBE cells were obtained from Shanghai Institute for Biological Science (Shanghai, China). All cells were grown in Roswell Park Memorial Institute-1640 (RPMI-1640) containing 10% fetal bovine serum (Gibco; Thermo Fisher Scientific, Inc.). All cell lines were cultured at 37˚C in an incubator containing a humidified (100%) atmosphere with 5% CO_2. To investigate the role of ferroptosis in ICC cells, 1 μM ferroptosis inhibitor ferrostatin-1 (Fer-1, cat. no. GC10380; GlpBio) was added for 24 h at 37˚C, as previously described (29).

Cell transfection. To overexpress wild-type (WT) luciferase reporter plasmids of hsa_circ_0050900 (pmirGLO-WT, Promega Corporation), mutant (MUT) luciferase reporter plasmids of hsa_circ_0050900, (pmirGLO-MUT, Promega Corporation), hsa-miR-605-3p, or inhibit the expression of hsa_circ_0050900 and hsa-miR-605-3p, Lipofectamine 2000 Transfection Reagent (Thermo Fisher Scientific, Inc.) was used for cell transfection for 4 h. Following digestion using 0.25% trypsin for 2 min at 37˚C, 1x10^5 cells were inoculated into 24-well plates and incubated overnight with 5% CO_2 at 37˚C. When the cell density was 80%, the medium was aspirated. A total of 0.5 μg (in 5 μl) plasmids, siRNAs, mimics, or inhibitors were dissolved in 250 μl OPTI-MEM (Gibco), then mixed in tube A. A total of 1.5 μl Lipofectamine 2000 was dissolved in 250 μl OPTI-MEM, mixed gently and stood for 5 min at room temperature in tube B. Tube B was added to tube A, mixed well, stood for 20 min at room temperature, then dropped into the 24-well plate well, mixed well, and cultured at 37˚C in 5% CO_2. After 4 h, the transfection medium was removed and 2 ml RPMI-1640 containing 10% fetal bovine serum) was added to continue culture for 24 or 48 h at 37˚C in 5% CO_2 before further investigation. Small interfering (si)-hsa_circ_0050900-1, hsa-miR-605-3p mimics, hsa-miR-605-3p inhibitor and negative control (NC) si-NC, miR-NC and NC inhibitor were synthesized by Shanghai GenePharma Co., Ltd. Sequences were as follows: si-hsa_circ_0050900-1 forward sequences, 5'-AUGCUGGAUGCAGAGGACCUU-3'; si-hsa_circ_0050900-1 reverse, 5'-AAGGUCCUCUGCAUCCAG CAU-3'; si-hsa_circ_0050900-2 forward sequences, 5'-AGA

GGACCUUCACGGCAUGGU-3'; si-hsa_circ_0050900-2 reverse, 5'-ACCAUGCCGUGAAGGUCCUCU-3'; si-hsa_circ_0050900-3 forward sequences, 5'-GCUGGAUGCAGAGGACCUUCA-3'; si-hsa_circ_0050900-3 reversed sequences, 5'-UGAAGGUCCUCUGCAUCCAGC-3'; si-NC forward sequences, 5'-GAGUACCGUUUAUGGCAGGAC-3'; si-NC reversed sequences, 5'-AGAGGACCUUCACGGCAUGGU-3'; hsa-miR-605-3p mimics forward sequences, 5'-AGAAGGCACUAUGAGAUUUAGAUU-3'; hsa-miR-605-3p mimics reversed sequences, 5'-UCUAAAUCUCAUAGUGCCUUCUUU-3'; hsa-miR-605-3p inhibitor, 5'-UCUAAAUCUCAUAGUGCCUUCU-3'; miR-NC forward, 5'-AAAGGUGUAGGAAAUUCACAUGUU-3'; miR-NC reverse, 5'-CAUGUGAAUUUCCUACACCUUUUU-3' and NC inhibitor, 5'-CAGUACUUUUGUGUAGUACAA-3'.

Clone formation assay. After cell counting, the cells were diluted to $1x10^4$ cell/ml, then $1x10^3$ cell/ml was inoculated on a 6-well plate (100 μl/well). After inoculation, complete medium was added (2 ml/well). After 1 week of culture at 37˚C in 5% CO_2, the medium was removed and cells were rinsed with PBS or normal saline twice for 10 sec each, fixed with 4% paraformaldehyde for 15 min at room temperature, washed with PBS twice for 10 sec each and 200 μl crystal violet staining solution was added to cover the bottom of the well. After incubation 20 min at room temperature, the 6-well plate was rinsed under running water for 10 sec and dried and the number of colonies (>50 cells) was calculated manually.

Cell migration assay. Transwell plate (8.0-μm pore size; Corning, Inc.) was used to performed cell migration assay. Cells in logarithmic growth phase were rinsed once with PBS and digested by 0.25% trypsin (for 2 min at 37˚C) into single cell suspension. Cell suspension was centrifuged at 550 x g for 5 min at 37˚C. After supernatant was aspirated and cells were suspended with RPMI-1640, cell concentration was adjusted to $1x10^6$/ml with RPMI-1640. A total of 100 μl cell suspension (in RPMI-1640) was added to the upper chamber of Transwell chamber and 600 μl RPMI-1640 containing 10% fetal bovine serum was added to the lower chamber. Following incubation for 48 h at 37˚C in 5% CO_2, cells in the upper chamber were removed and wiped with cotton swabs. Cells were fixed with 4% paraformaldehyde for 15 min at 37˚C, washed with PBS once for 30 sec, stained with 1% crystal violet for 10 min at room temperature and washed with PBS once for 30 sec. Migrated cells were observed under a light microscope (200x).

Bioinformatics prediction and dual-luciferase reporter gene assay. University of California-Santa Cruz (UCSC, genome.ucsc.edu/; version: GRCh37/hg19) combined with circPrimer 2.0 (https://www.bio-inf.cn/) was utilized to analyze the source of hsa_circ_0050900. CircAtlas 2.0 (https://ngdc.cncb.ac.cn/circatlas/) predicted the binding sequence between hsa_circ_0050900 and hsa-miR-605-3p. TargetScanHuman 7.1 (targetscan.org/vert_71/) predicted the binding sites of hsa-miR-605-3p and SLC3A2 3' untranslated region (UTR). For dual-luciferase reporter gene assay, 293T cells were plated in 24-well plates ($5x10^4$ cells/well) and transfected with WT or MUT luciferase reporter plasmids and hsa-miR-605-3p mimics using Lipofectamine 2000 Transfection Reagent (Thermo Fisher Scientific, Inc.). Following transfected for 48 h, luciferase activity was detected using a luciferase reporter kit (cat. no. FR201-01; TransGen Biotech Co., Ltd.). Luciferase activity was calculated as activity of firefly luciferase activity compared with Renilla luciferase activity. WT and MUT plasmid containing hsa_circ_0050900 (WT1, 5'-TGGAAGGATGGTCTTGCCTTCA-3'; MUT1, 5'-TGGCGAGGGATTTTAGCATCCT-3'; WT2, 5'-ACCAACCTGAACAATGCCTTCG-3' and MUT2, 5'-CCGTGCCAACCCACAATGATAT-3') and SLC3A2 3' UTR sequence (WT, 5'-AAATAGGGTGTTTTCTGCCTTCA-3' and MUT, 5'-GGTAACATTGGCTATATCCTGTT-3') were inserted into pmirGLO plasmid (Promega Corporation).

Fluorescence in situ hybridization (FISH). As previously described (30), subcellular localization of hsa_circ_0050900 was detected using a FISH kit for digoxigenin (cat. no. BIS-P0001; Guangzhou Bersin Co., Ltd.). HuCCT-1 cells were fixed by 4% paraformaldehyde for 15 min at 25˚C, washed with PBS three times (5 min/time), and treated 0.1% TritonX-100 for 15 min at 25˚C. After wash with PBS for twice (5 min/time), slides was incubated in hybridization buffer (Wuhan Servicebio Technology CO., LTD., Wuhan, China) for 1 h at 37˚C. Then, slides were treated with digoxigenin-labeled hsa_circ_0050900 probe (cDNA, 5'-CCGTGAAGGTCCTCTGCATC-3', 20 nt; Wuhan Servicebio technology CO., LTD.; diluted to 40 nM with hybridization buffer and denaturation at 73˚C for 5 min) hybridized at 37˚C for 16 h, soaked in 2X saline sodium citrate buffer for 10 min at 37˚C, twice in 1X saline sodium citrate buffer for 5 min at 37˚C and twice in 0.5X saline sodium citrate buffer for 5 min at 37˚C. Then, slides were incubated in normal rabbit serum (1:20 in PBS; cat. no. G1209; Wuhan Servicebio technology CO., LTD.) for 30 min at 25˚C and incubated anti-DIG-HRP (dilution: 1:1,000; cat. no. 200-032-156; Jackson Immuno Research Europe, Ltd.) for 50 min at 37˚C, soaked in PBS thrice (5 min/time). Slides incubated with iF647-Tyramide (1:500; cat. no. G1232; Wuhan Servicebio technology CO., LTD.) for 10 min at 25˚C, and washed using TBST (0.05% Tween-20) thrice (3 min/time) at 25˚C and stained with DAPI for 10 min at 25˚C. Slides were observed under a Zeiss LSM880 NLO confocal microscope (Leica GmbH, 1,000x) with Zen Black software 2.0 (Carl Zeiss Microscopy GmbH).

Reverse transcription-quantitative PCR (RT-qPCR) and Sanger sequencing. RNA was isolated from cells using TRIzol reagent (Thermo Fisher Scientific, Inc.). Total RNA underwent RT (RT kit, cat. no. K1622, Thermo Fisher Scientific, Inc.) and qPCR detection was performed using SYBR-Green (cat. no. P122; Vazyme Biotech Co., Ltd.). For RT, 1 μl total RNA (100 ng), 1 μl oligo (dT)18 for circRNA or mRNA expression or hsa-miR-605-3p RT primer (100 μM) for expression of hsa-miR-605-3p and 10 μl nuclease-free water were mixed gently, centrifuged at 250 x g for 5 sec at 25˚C and incubated at 65˚C for 5 min. A total of 4 μl 5X Reaction Buffer, 1 μl RiboLock RNase Inhibitor (20 U/μl), 2 μl 10 mM dNTP Mix and 1 μl RevertAid M-MuLV RT (200 U/μl) were mixed gently and centrifuged 250 x g for 5 sec at 25˚C, followed by incubation for 60 min at 42˚C. The reaction was terminated by heating at 70˚C for 5 min. Thermocycling conditions were

as follows: Initial denaturation for 30 sec at 95˚C, followed by 40 cycles of 30 sec at 95˚C and 1 min at 72˚C. GAPDH or U6 (Gene ID 26827) was used as an internal reference and $2^{-\Delta\Delta Cq}$ was used to calculate the relative expression (31). Primers were designed by Primer Premier 5 and synthesized by Shanghai Sangon Pharmaceutical Co., Ltd. In addition, qPCR products were analyzed by Sanger sequencing to confirm the presence of hsa_circ_0050900 circularization site. The primer sequences were as follows: hsa_circ_0050900 forward, 5'-GTCTTG CCTTCAATGCCCTG-3' and reverse, 5'-CATGCCGTGAAG GTCCTCTG-3'; hsa-miR-605-3p RT primer, 5'-GTCGTA TCCAGTGCAGGGTCCGAGGTATTCGCACTGGATACG ACTCTAAA-3'; hsa-miR-605-3p forward, 5'-AGAAGGCAC TATGAGATTTAGA-3' and reverse, 5'-GTGCAGGGTCCG AGGT-3'; SLC3A2 forward, 5'-ATGGAGCTACAGCCTCCT GA-3' and reverse, 5'-CGCGCTGAGACCCTGG-3'; GAPDH forward, 5'-GAAGGTGAAGGTCGGAGTC-3' and reverse, 5'-GAAGATGGTGATGGGATTTC-3' and U6 forward, 5'-CTC GCTTCGGCAGCACA-3' and reverse, 5'-AACGCTTCACGA ATTTGCGT-3'.

Western blot. Total cell protein was extracted with RIPA lysis buffer (cat. no. P0013B; Beyotime Institute of Biotechnology) and quantified using BCA protein concentration assay kit (cat. no. BL521A; Biosharp Life Sciences). Protein (20 μg/lane) was separated by 10% SDS-PAGE, transferred onto PVDF membrane, blocked using 5% skimmed milk for 2 h at 25˚C and incubated with primary antibodies as follows: GPX4 (cat. no. 14432-1-AP; Proteintech Group, Inc.; 1:6,000), SLC3A2 (cat. no. 66883-1-Ig; Proteintech Group, Inc.; 1:100,000) and GAPDH (cat. no. 10494-1-AP; Proteintech Group, Inc.; 1:20,000) at 4˚C overnight. HRP-conjugated Affinipure Goat Anti-Mouse IgG (H+L; cat. no. SA00001-1; Proteintech Group, Inc.; 1:10,000) and Anti-Rabbit IgG (H+L; cat. no. SA00001-2; Proteintech Group, Inc.; 1:10,000) secondary antibodies were incubated at room temperature for 2 h. GAPDH was used as an internal reference and exposure was performed using an ultra-sensitive ECL chemiluminescent substrate (cat. no. BL520A; Biosharp Life Sciences). Image J 1.48v (National Institutes of Health, Bethesda, MD, USA) was used for densitometry.

Detection of Fe^{2+} and reactive oxygen species (ROS) levels. Iron (cat. no. #MAK025; MilliporeSigma) and ROS assay kit (cat. no. #S0033S; Beyotime Institute of Biotechnology) were used to measure Fe^{2+} and ROS levels in HuCCT-1 cells, respectively, according to the manufacturer's instructions.

Subcellular fractionation assay. The subcellular localization of hsa_circ_0050900 was verified using a cytoplasmic and nuclear RNA purification kit (cat. no. #21000; Norgen Biotek Corp.). ICC cells ($5x10^6$) were treated with 200 μl freezing cell isolation buffer for 5 min to separate the cytoplasm and nuclei. RT-qPCR was used to measure hsa_circ_0050900 expression in the cytoplasm and nucleus as aforementioned.

RNA immunoprecipitation (RIP) assay. EZ-Magna RIP RNA Binding Protein Immunoprecipitation kit (cat. no. #17-701; EMD Millipore) was used according to the manufacturer's instructions. After cells were lysed in complete RIP lysis buffer, whole cell lysate was collected and treated with conjugated anti-AGO2 (cat. no. #67934-1-Ig; Proteintech Group, Inc.; 5 μg) or normal mouse IgG overnight at 4˚C. Next, 10 μl whole cell lysate was used as input (positive control) and IgG acted as negative control. The immunoprecipitated RNA was extracted and relative enrichment of hsa_circ_0050900 and SLC3A2 in immunoprecipitated RNA was detected by RT-qPCR as aforementioned.

Statistical analysis. SPSS 16.0 software (SPSS, Inc.) was used for statistical analysis. All experiments were repeated three times. Data are expressed as the mean ± standard deviation. Unpaired t test or one-way ANOVA followed by Tukey's post hoc test was used to analyze data. $P<0.05$ was considered to indicate a statistically significant difference.

Results

hsa_circ_0050900 is derived from ACTN4 gene and is highly expressed in ICC cells. UCSC combined with circPrimer was used to analyze the source of hsa_circ_0050900. hsa_circ_0050900 was derived from ACTN4 gene (Fig. 1A). Sanger sequencing showed that there was a back-splice junction for hsa_circ_0050900 (Fig. 1B), which confirmed the circular structure of hsa_circ_0050900. Next, hsa_circ_0050900 expression in ICC cells was measured relative to GAPDH. hsa_circ_0050900 was elevated in ICC cells and highest in HuCCT-1 cells (Fig. 1C). Therefore, HuCCT-1 cells were selected for subsequent experiments.

Knockdown of hsa_circ_0050900 suppresses proliferation and migration by promoting ICC cell ferroptosis. To explore the function of hsa_circ_0050900, specific interference fragments were designed for hsa_circ_0050900. qPCR results showed si-hsa_circ_0050900-1, si-hsa_circ_0050900-2 and si-hsa_circ_0050900-3 interfered with expression of hsa_circ_0050900 and si-hsa_circ_0050900-3 had highest interference efficiency (Fig. 2A) . Therefore, si-hsa_circ_0050900-3 was selected for subsequent experiments. To investigate whether hsa_circ_0050900 was involved in ferroptosis, HuCCT-1 cells were treated with ferroptosis inhibitor Fer-1 following transfection of si-NC or si-hsa_circ_0050900-3. Fe^{2+} and ROS levels were promoted after knocking down hsa_circ_0050900, while Fe^{2+} and ROS levels were suppressed by Fer-1 (Fig. 2B and C). In addition, ferroptosis-associated factor GPX4 expression was suppressed after hsa_circ_0050900 was knocked down; this effect on GPX4 expression was reversed by Fer-1 treatment (Fig. 2D). Cell proliferation and migration were suppressed after knocking down hsa_circ_0050900 expression, while these phenomenon were reversed by Fer-1 treatment (Fig. 2E and F). Collectively, inhibition of hsa_circ_0050900 inhibited proliferation and migration by promoting ICC cell ferroptosis.

hsa_circ_0050900 negatively regulates hsa-miR-605-3p. To explore the potential mechanism of hsa_circ_0050900, the present study confirmed the localization of hsa_circ_0050900. FISH showed that hsa_circ_0050900 was mainly localized in cytoplasm in HuCCT-1 cells (Fig. 3A). RT-qPCR verified hsa_circ_0050900 was primarily located in cytoplasm (Fig. 3B). Then, the expression was detected after knocking

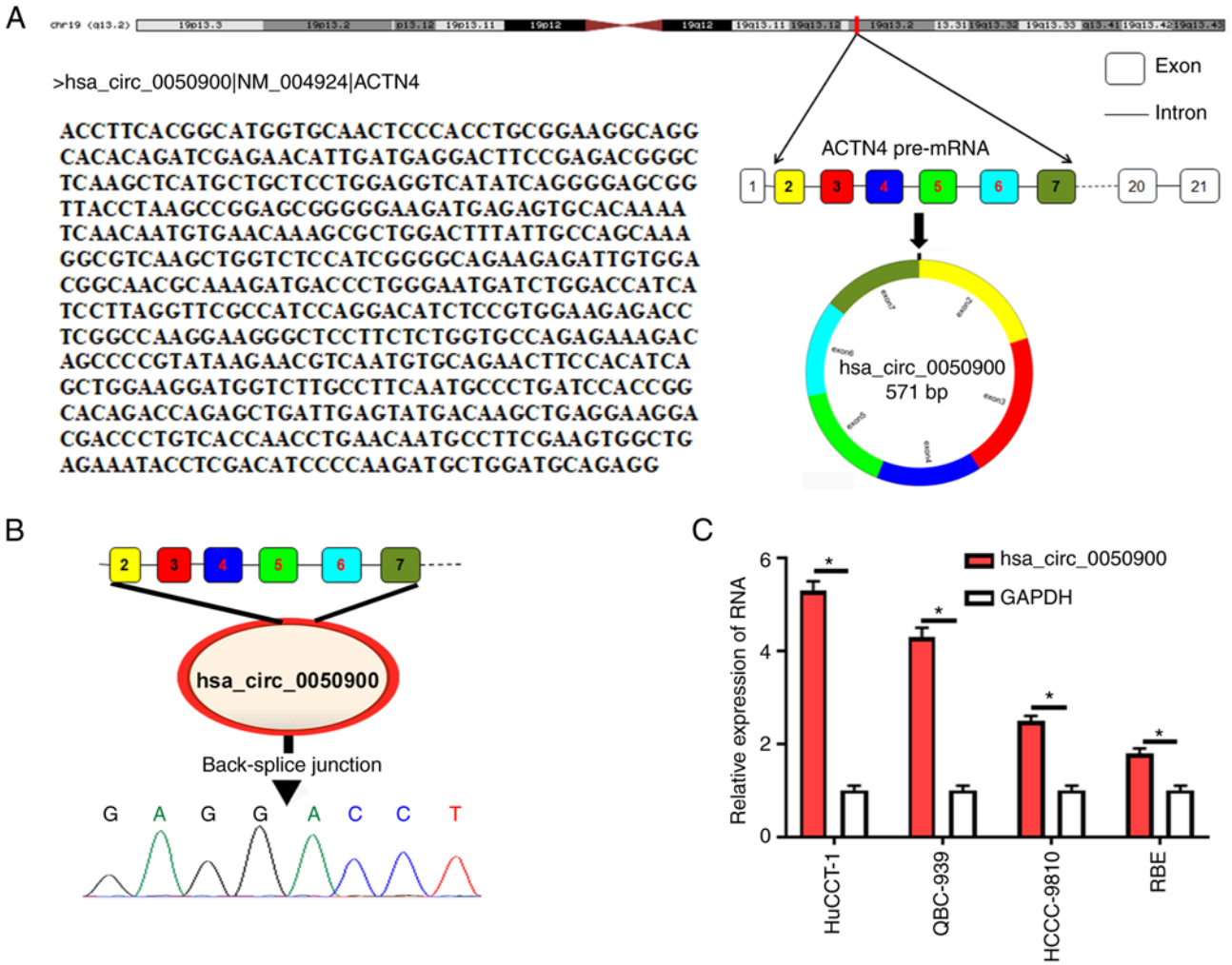

Figure 1. hsa_circ_0050900 is derived from ACTN4 gene and is highly expressed in ICC cells. (A) UCSC combined with circPrimer was used to analyze the source of hsa_circ_0050900. (B) Sanger sequencing of the hsa_circ_0050900 circularization site. (C) Reverse transcription-quantitative PCR detection of hsa_circ_0050900 expression in human ICC-derived HuCCT-1, QBC-939, HCCC-9810 and RBE cells. *P<0.05. ACTN4, actinin α4; ICC, intrahepatic cholangiocarcinoma; UCSC, University of California-Santa Cruz; circ, circular.

down expression of hsa_circ_0050900. qPCR indicated that hsa-miR-605-3p expression was elevated after knockdown of hsa_circ_0050900 (Fig. 3C). CircAtlas 2.0 software was used to predict the binding sequence between hsa_circ_0050900 and hsa-miR-605-3p. There were two binding sites between hsa_circ_0050900 and hsa-miR-605-3p (Fig. 3D). Dual-luciferase reporter gene assay demonstrated that only hsa-miR-605-3p mimics decreased the luciferase activity of hsa_circ_0050900 WT but not hsa_circ_0050900 MUT (Fig. 3E). AGO2-RIP assays revealed hsa_circ_0050900 expression was promoted by hsa-miR-605-3p mimics (Fig. 3F). These results indicated that hsa_circ_0050900 regulated hsa-miR-605-3p expression (Fig. 3E and F). hsa_circ_0050900 negatively regulated hsa-miR-605-3p expression.

hsa-miR-605-3p targets SLC3A2. To study hsa-miR-605-3p function, hsa-miR-605-3p mimics or miR-NC was transfected into HuCCT-1 cells. Compared with miR-NC, hsa-miR-605-3p expression was significantly elevated after transfection with hsa-miR-605-3p mimics, which indicated successful overexpression of hsa-miR-605-3p (Fig. 4A). Overexpression of hsa-miR-605-3p inhibited the mRNA and protein expression of SLC3A2 (Fig. 4A and B). Then, TargetScanHuman 7.1 software was used to predict the binding site between SLC3A2 3'UTR and hsa-miR-605-3p (Fig. 4C). Dual-luciferase reporter gene assay demonstrated hsa-miR-605-3p mimics decreased the luciferase activity of SLC3A2 3'UTR WT, but not SLC3A2 3'UTR MUT (Fig. 4D). Additionally, AGO2-RIP assay showed hsa-miR-605-3p mimics increased expression of SLC3A2, but not miR-NC (Fig. 4E). These results verified that hsa-miR-605-3p could regulate SLC3A2 expression.

Overexpression of hsa-miR-605-3p targets SLC3A2 to promote ICC cell ferroptosis and inhibit proliferation and migration. Fe^{2+} and ROS levels were increased by hsa-miR-605-3p mimics compared with miR-NC (Fig. 5A and B). Moreover, following overexpression of hsa-miR-605-3p, GPX4 protein expression was suppressed in comparison with miR-NC group (Fig. 5C). Cell function experiments demonstrated overexpression of hsa-miR-605-3p reduced proliferation and migration in comparison with miR-NC (Fig. 5D and E). Overexpression of hsa-miR-605-3p targeted SLC3A2 to promote ICC cell ferroptosis and inhibit proliferation and migration.

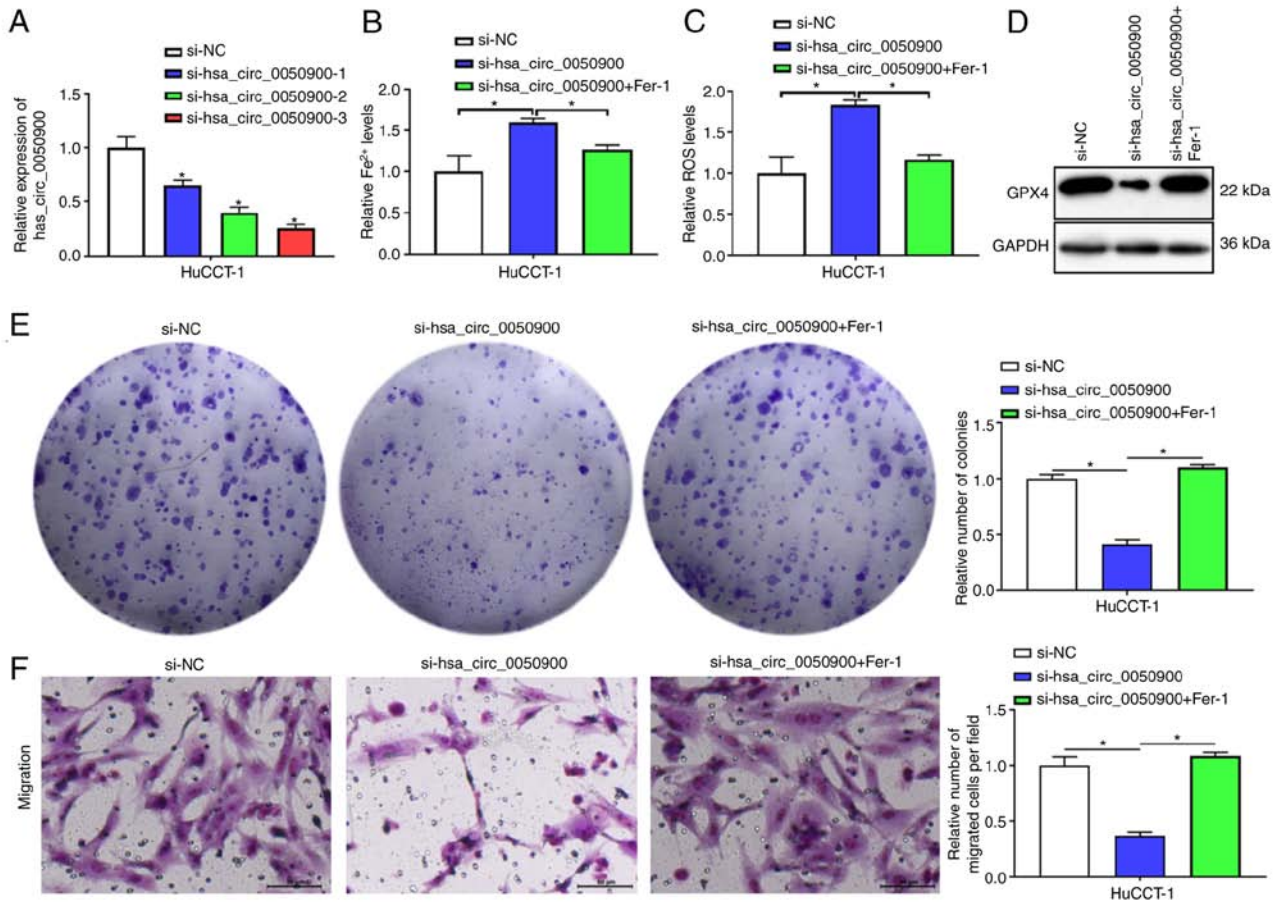

Figure 2. Knockdown of hsa_circ_0050900 suppresses proliferation and migration by promoting ICC cell ferroptosis. (A) si-NC, si-hsa_circ_0050900-1, si-hsa_circ_0050900-2 and si-hsa_circ_0050900-3 were transfected into HuCCT-1 cells for 24 h and cells were collected for reverse transcription-quantitative PCR. si-hsa_circ_0050900-1, si-hsa_circ_0050900-2, si-hsa_circ_0050900-3 showed knockdown effect for hsa_circ_0050900 expression. A total of 1 μM ferroptosis inhibitor Fer-1 was added for 24 h, then cells were collected for further analysis. (B) Iron assay kit was used to evaluate Fe^{2+} levels. (C) ROS assay kit was used to assess ROS levels. (D) Western blot detection of GPX4 protein. (E) Clone formation assay was used to measure proliferation. (F) Transwell assay was used to detect migration. n=3. Magnification, 200 x; Scale bar, 50 μm. *P<0.05 vs. si-NC. circ, circular; ICC, intrahepatic cholangiocarcinoma; si-NC, small interfering negative control; Fer-1, ferrostatin-1; ROS, reactive oxygen species; GPX4, glutathione peroxidase 4.

hsa_circ_0050900 regulates SLC3A2 expression via hsa-miR-605-3p. hsa-miR-605-3p expression was knocked down in HuCCT-1 cells using hsa-miR-605-3p inhibitor. hsa-miR-605-3p inhibitor decreased the expression of hsa-miR-605-3p relative to NC inhibitor, indicating that hsa-miR-605-3p inhibitor had an interfering effect (Fig. 6A). mRNA and protein levels of the downstream target gene SLC3A2 of hsa-miR-605-3p were suppressed after knocking down hsa_circ_0050900 (Fig. 6B and C). However, knocking down hsa-miR-605-3p attenuated the decrease in SLC3A2 mRNA and protein expression induced by inhibition of hsa_circ_0050900 (Fig. 6B and C). These results indicated that hsa_circ_0050900 regulated SLC3A2 expression via hsa-miR-605-3p.

hsa_circ_0050900 regulates SLC3A2 expression via sponging hsa-miR-605-3p to affect ICC cell ferroptosis, proliferation and migration. Finally, the effects of hsa_circ_0050900 and hsa-miR-605-3p on cell ferroptosis, proliferation and migration were assessed. Knocking down hsa-miR-605-3p reduced the increases of Fe^{2+} and ROS induced by inhibition of hsa_circ_0050900 (Fig. 7A and B). hsa-miR-605-3p inhibitor decreased the downregulation of GPX4 caused by knocking down hsa_circ_0050900 (Fig. 7C). hsa-miR-605-3p inhibitor attenuated the decrease in cell proliferation and migration caused by knocking down hsa_circ_0050900 (Fig. 7D and E). Taken together, hsa_circ_0050900 regulated SLC3A2 expression via sponging hsa-miR-605-3p to affect ICC cell ferroptosis, proliferation and migration.

Discussion

Despite technological advances and multimodal treatment approaches, ICC prognosis remains poor due to frequent delays in diagnosis (32). Therefore, exploring the molecular pathogenesis of ICC is helpful to provide targets for diagnosis and treatment. The present study explored the mechanism of action of hsa_circ_0050900 in ferroptosis in ICC cells *in vitro*. hsa_circ_0050900 affected ICC cell ferroptosis by targeting hsa-miR-605-3p to regulate SLC3A2.

circRNAs are a class of ncRNAs that play vital roles in cancer biology (33). circRNA nuclear factor I B inhibits tumor growth and metastasis by inhibiting the MEK1/ERK pathway in ICC (34). Jiang *et al* (35) validated in clinical tissues that circRNA CDR1 antisense RNA may serve as a

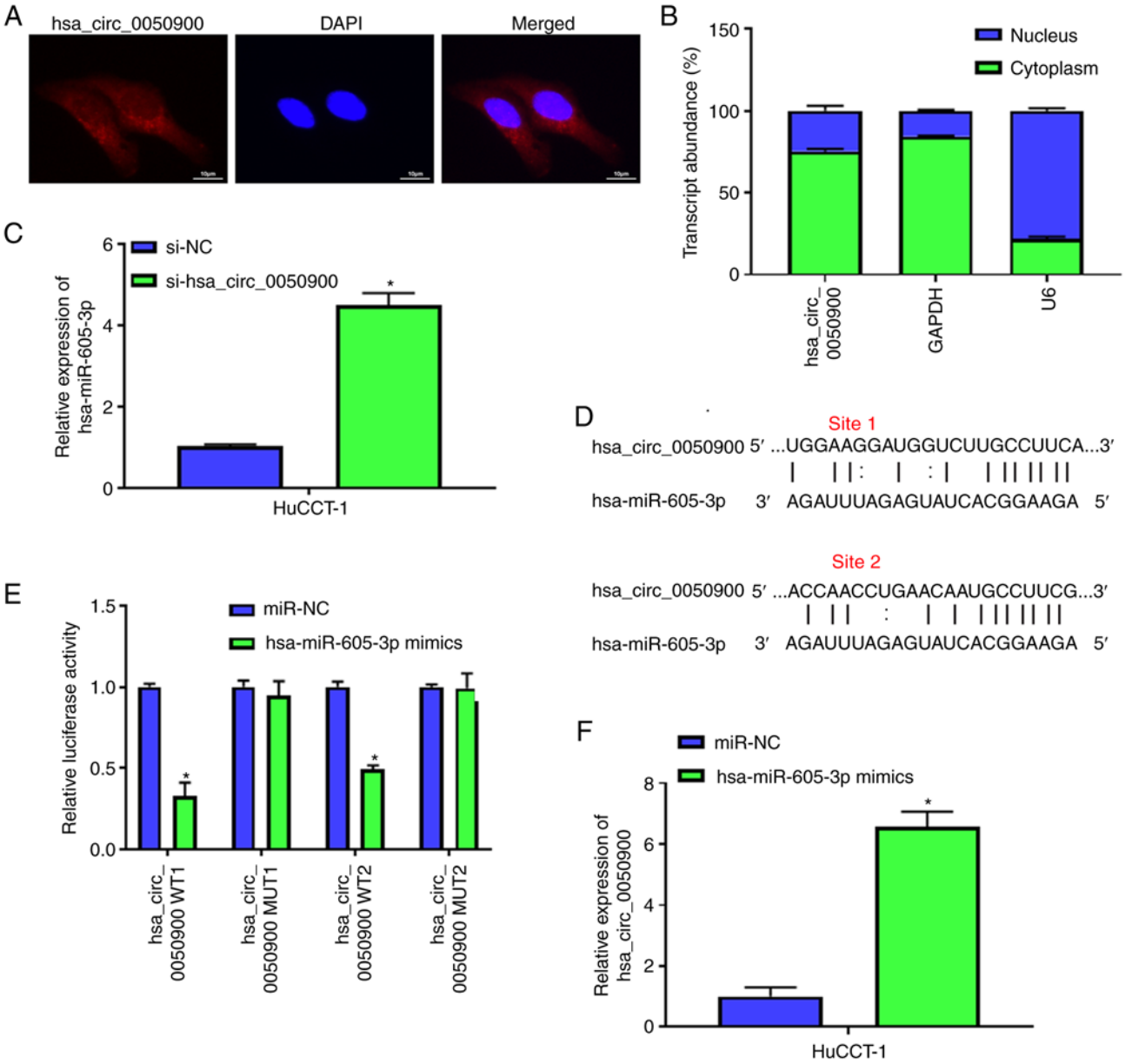

Figure 3. hsa_circ_0050900 negatively regulates hsa-miR-605-3p. (A) Fluorescence in situ hybridization verification of the distribution of hsa_circ_0050900 in HuCCT-1. magnification, 1000 x; Scale bar, 10 μm. (B) Cytoplasmic and nuclear RNA purification kit was used to separate the cytoplasm and nuclei and RT-qPCR was used to measure hsa_circ_0050900, GAPDH and U6 expression in the cytoplasmic and nucleus. (C) si-hsa_circ_0050900-3 or si-NC was transfected into HuCCT-1 cells for 24 h and cells were collected for RT-qPCR detection of hsa-miR-605-3p. (D) CircAtlas 2.0 software was used to predict binding sequence between hsa_circ_0050900 and hsa-miR-605-3p. (E) Wild-type or mutant luciferase reporter plasmid and hsa-miR-605-3p mimics or miR-NC were co-transfected into 293T cells for 48 h and cells were collected for dual-luciferase reporter gene assay to confirm the binding regulatory association between hsa_circ_0050900 and hsa-miR-605-3p. (F) hsa-miR-605-3p mimics or miR-NC was transfected into HuCCT-1 cells for 48 h and cells were collected for AGO2-RIP assay to detect changes in binding of hsa-miR-605-3p to hsa_circ_0050900. *P<0.05 vs. miR-NC. circ, circular; miR, microRNA; RT-q, reverse transcription-quantitative; si-NC, small interfering negative control; AGO2-RIP, argonaute2-RNA immunoprecipitation.

potential malignant molecular biomarker to predict aggressive tumor progression and poor prognosis in patients with cholangiocarcinoma. Chen *et al* (14) reported elevated circACTN4 expression is associated with enhanced tumor proliferation and metastasis *in vitro* and *in vivo* and poor prognosis after ICC resection. The present *in vitro* experiments demonstrated that hsa_circ_0050900 was derived from ACTN4 gene and was highly expressed in ICC cells. In addition, inhibition of hsa_circ_0050900 suppressed proliferation and migration by promoting ICC cell ferroptosis. The present study showed that hsa_circ_0050900 affected the migration of ICC.

Competing endogenous RNAs (ceRNAs) have been studied in ICC. Zhou *et al* (36) revealed functional long non-coding RNAs (lncRNAs) in ICC through comprehensive analysis of ceRNA networks, providing a novel strategy for subsequent functional studies of lncRNAs in ICC. Kang *et al* (37) predicted the relationship between the central gene-associated ceRNA network and overall survival of patients with ICC from transcriptome sequencing data. There are also related studies on ceRNAs in circRNA/miR/mRNA networks: Xu *et al* (38) reported circRNA 3-hydroxy-3-methylglutaryl-CoA synthase 1-016 regulates CD73 and galectin

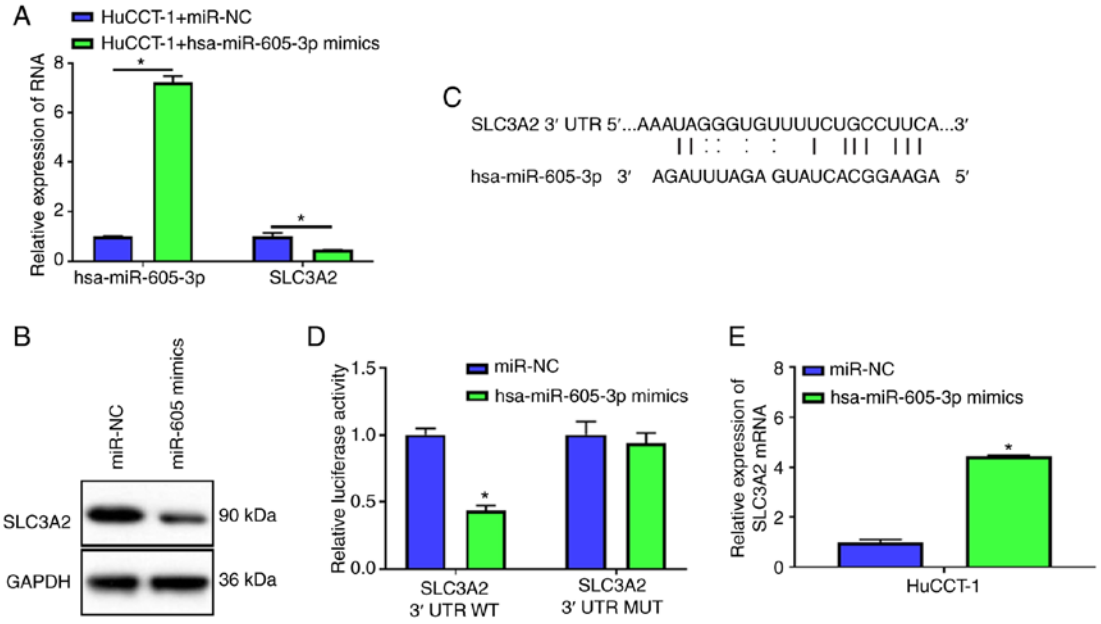

Figure 4. hsa-miR-605-3p targets SLC3A2. (A) hsa-miR-605-3p mimics or miR-NC was transfected into HuCCT-1 cells for 24 h and cells were collected for reverse transcription-quantitative PCR detection of hsa-miR-605-3p and SLC3A2 mRNA expression. (B) Western blot determination of SLC3A2 protein expression. n=3. (C) TargetScanHuman 7.1 software predicted the binding site of hsa-miR-605-3p and SLC3A2 3' UTR. (D) WT or MUT luciferase reporter plasmids and hsa-miR -605-3p mimics or miR-NC were co-transfected into 293T cells for 48 h and cells were collected for dual-luciferase reporter gene assay to confirm the binding regulatory relationship between SLC3A2 3' UTR and hsa-miR-605-3p. (E) Changes in the binding of hsa-miR-605-3p to SLC3A2 mRNA following overexpression of hsa-miR-605-3p in HuCCT-1 cells were verified by AGO2-RIP assay. *P<0.05 vs. miR-NC. miR, microRNA; SLC3A2, solute carrier family 3 member 2; NC, negative control; UTR, untranslated region; WT, wild-type; MUT, mutant.

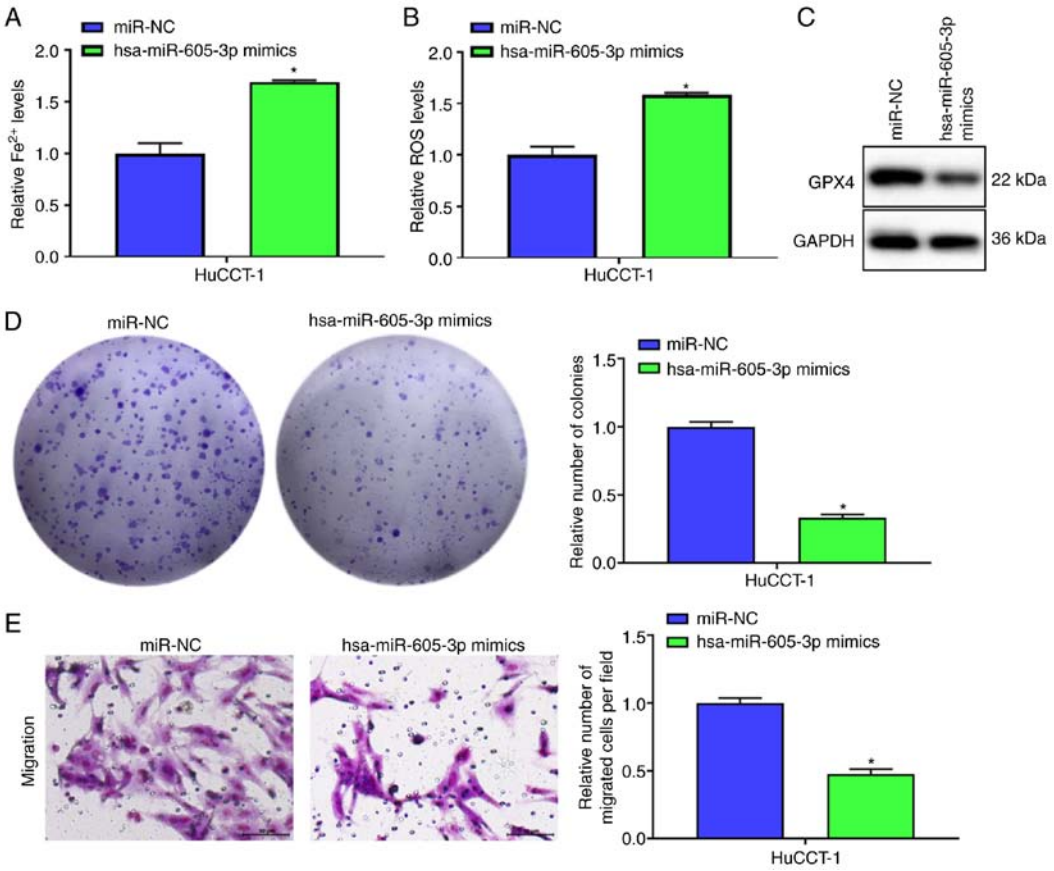

Figure 5. Overexpression of hsa-miR-605-3p targets SLC3A2 to promote ICC cell ferroptosis and inhibit proliferation and migration. hsa-miR-605-3p mimics or miR-NC was transfected into HuCCT-1 for 48 h. (A) Iron assay kit was used to assess Fe^{2+} levels. (B) ROS assay kit was used to determine ROS levels. (C) Western blot detection of GPX4 protein. (D) Clone formation assay was used to evaluate proliferation. (E) Transwell assay was used to detect migration. n=3. Magnification, 200 x; Scale bar, 50 μm. *P<0.05 vs. miR-NC. miR, microRNA; SLC3A2, solute carrier family 3 member 2; ICC, intrahepatic cholangiocarcinoma; NC, negative control; ROS, reactive oxygen species; GPX4, glutathione peroxidase 4.

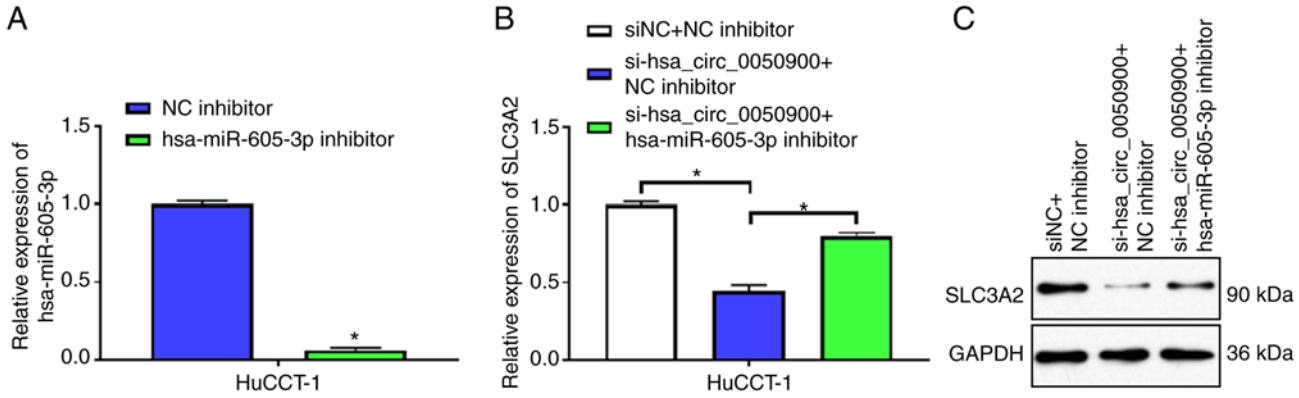

Figure 6. hsa_circ_0050900 regulates SLC3A2 expression via hsa-miR-605-3p. (A) hsa-miR-605-3p inhibitor or NC inhibitor was transfected into HuCCT-1 cells for 24 h. RT-qPCR detection of the interference effect of hsa-miR-605-3p inhibitor. *P<0.05 vs. NC inhibitor. (B) si-hsa_circ_0050900-3 and hsa-miR-605-3p inhibitor or NC inhibitor were co-transfected into HuCCT-1 cells for 24 h. RT-qPCR determination of SLC3A2 mRNA expression. (C) si-hsa_circ_0050900-3 and hsa-miR-605-3p inhibitor or NC inhibitor were transfected into HuCCT-1 cells for 48 h. Western blot detection of SLC3A2 protein expression. n=3. circ, circular; SLC3A2, solute carrier family 3 member 2; miR, microRNA; RT-q, reverse transcription-quantitative; si, small interfering; NC, negative control.

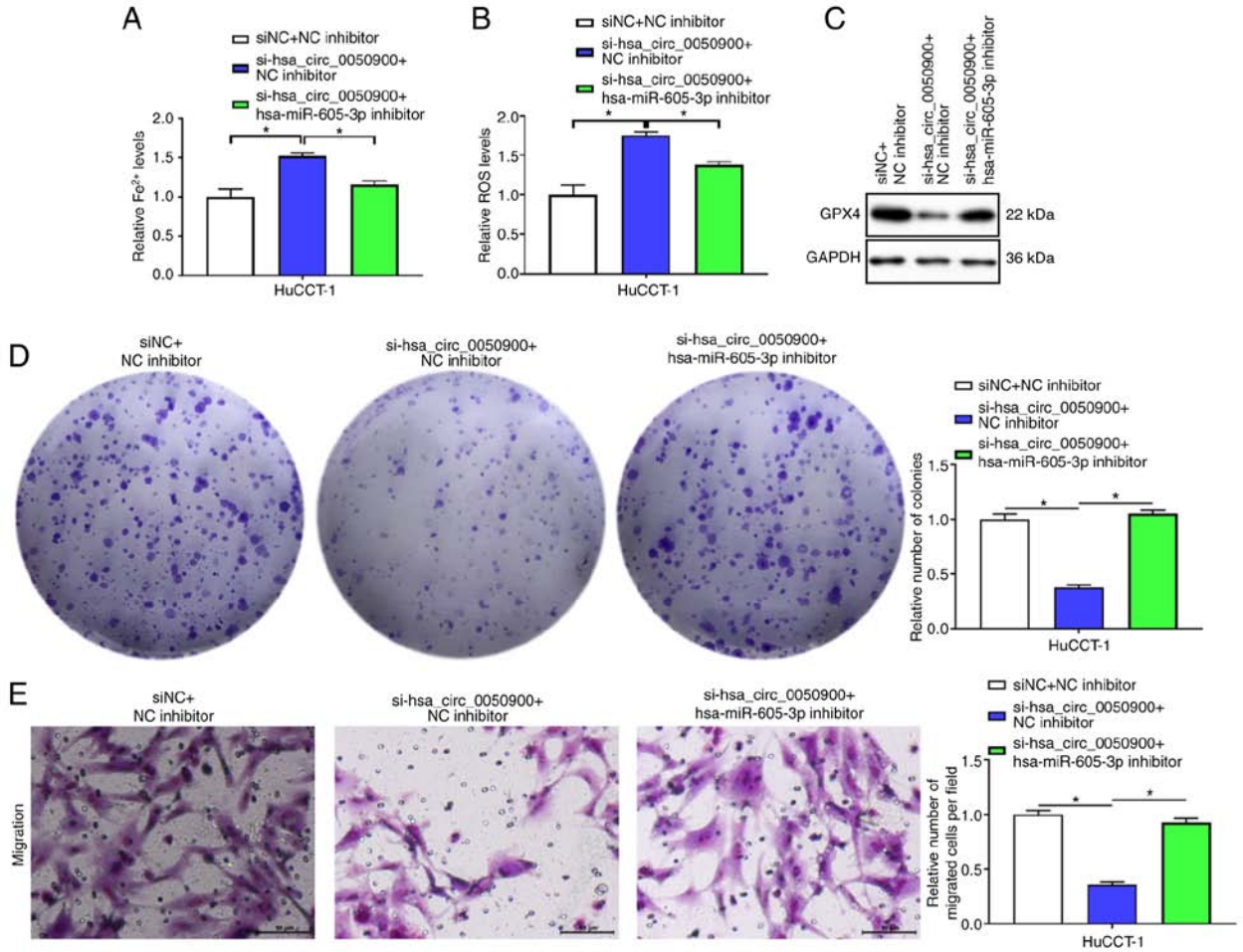

Figure 7. hsa_circ_0050900 regulates SLC3A2 expression via sponging hsa-miR-605-3p to affect intrahepatic cholangiocarcinoma cell ferroptosis, proliferation and migration. si-hsa_circ_0050900-3 and hsa-miR-605-3p inhibitor or NC inhibitor were co-transfected into HuCCT-1 cells for 48 h. (A) Iron assay kit was used to monitor Fe^{2+} levels. (B) ROS assay kit was used to examine ROS levels. (C) Western blot measurement of GPX4 protein. (D) Clone formation assay was used to test proliferation. (E) Transwell assay was used to assess migration. n=3. magnification, 200 x; Scale bar, 500 μm. *P<0.05. circ, circular; SLC3A2, solute carrier family 3 member 2; miR, microRNA; NC, negative control; si, small interfering; ROS, reactive oxygen species; GPX4, glutathione peroxidase 4.

8 by sponging miR-1236-3p to induce ICC cell invasion and tumor immune microenvironment remodeling. Tang *et al* (39) found circRNA reticulon 4 interacting protein 1 regulates the malignant progression of ICC by sponging miR-541-5p to induce hypoxia-inducible factor 1A production. These studies revealed a network of ICC-specific ceRNAs. Here,

hsa_circ_0050900 negatively regulated hsa-miR-605-3p. In addition, hsa-miR-605-3p targeted SLC3A2. This suggests that hsa_circ_0050900/hsa-miR-605-3p/SLC3A2 signaling functions in ICC through a ceRNA mechanism.

SLC3A2 serves a key role in amino acid and glucose cellular nutrition, redox homeostasis and nucleotide availability, which are all critical for cell proliferation (40). There is increasing evidence that SLC3A2 is upregulated in a variety of cancers and is associated with tumor growth (19,41). Decreased expression of SLC3A2 inhibits osteosarcoma cell proliferation through G2/M arrest (42). In hepatocellular carcinoma, overexpressed lncRNA small nucleolar RNA host gene 1 activates the Akt pathway by regulating SLC3A2, resulting in sorafenib resistance (43). In cholangiocarcinoma, Janpipatkul *et al* (44) reported inhibition of cell invasion and migration in L-type amino acid transporter 1 knockdown KKU-M213 cells may be mediated in part by upregulating miR-7 to inhibit the SLC3A2 pathway. Here, overexpression of hsa-miR-605-3p targeted SLC3A2 to promote ICC cell ferroptosis and inhibit proliferation and migration. hsa_circ_0050900 affected ICC cell ferroptosis, proliferation and migration by regulating SLC3A2 expression via sponging hsa-miR-605-3p. To the best of our knowledge, the present study is the first to report the targeted regulatory association between hsa-miR-605-3p and SLC3A2 in ICC.

The present study confirmed hsa_circ_0050900 was highly expressed in ICC cells. Furthermore, the present study conducted a preliminary exploration of the mechanism involved in hsa_circ_0050900. *In vitro* experiments found hsa_circ_0050900 affected ICC cell ferroptosis by targeting hsa-miR-605-3p to regulate SLC3A2. This may provide new ideas and targets for treating ICC. However, these effects should be studied in animal models and expression of hsa_circ_0050900, has-miR-605-3p and SLC3A2 should be validated in ICC clinical samples and correlation analysis should be performed.

Acknowledgements

Not applicable.

Funding

This work was funded by the National Science Foundation of China (grant no. 82002587).

Availability of data and materials

The datasets used and/or analyzed during the current study are available from the corresponding author on reasonable request.

Authors' contributions

SQ and LZ conceived and designed the study. XS and JY performed experiments and acquired the data. LX and MW analyzed and interpreted the data. JY performed statistical analysis. XS wrote the manuscript. LZ and XS revised the manuscript. LZ and SQ confirm the authenticity of all the raw data. All authors have read and approved the final manuscript.

Ethics approval and consent to participate

Not applicable.

Patient consent for publication

Not applicable.

Competing interests

The authors declare that they have no competing interests.

References

1. Kelley RK, Bridgewater J, Gores GJ and Zhu AX: Systemic therapies for intrahepatic cholangiocarcinoma. J Hepatol 72: 353-363, 2020.
2. Rahnemai-Azar AA, Weisbrod A, Dillhoff M, Schmidt C and Pawlik TM: Intrahepatic cholangiocarcinoma: Molecular markers for diagnosis and prognosis. Surg Oncol 26: 125-137, 2017.
3. Moris D, Palta M, Kim C, Allen PJ, Morse MA and Lidsky ME: Advances in the treatment of intrahepatic cholangiocarcinoma: An overview of the current and future therapeutic landscape for clinicians. CA Cancer J Clin 73: 198-222, 2023.
4. Aoki S, Inoue K, Klein S, Halvorsen S, Chen J, Matsui A, Nikmaneshi MR, Kitahara S, Hato T, Chen X, *et al*: Placental growth factor promotes tumour desmoplasia and treatment resistance in intrahepatic cholangiocarcinoma. Gut 71: 185-193, 2022.
5. Hewitt DB, Brown ZJ and Pawlik TM: Surgical management of intrahepatic cholangiocarcinoma. Expert Rev Anticancer Ther 22: 27-38, 2022.
6. Chen Z, Jiang J, Fu N and Chen L: Targetting ferroptosis for blood cell-related diseases. J Drug Target 30: 244-258, 2022.
7. Lei G, Zhuang L and Gan B: Targeting ferroptosis as a vulnerability in cancer. Nat Rev Cancer 22: 381-396, 2022.
8. Chen J, Li X, Ge C, Min J and Wang F: The multifaceted role of ferroptosis in liver disease. Cell Death Differ 29: 467-480, 2022.
9. Li D, Wang Y, Dong C, Chen T, Dong A, Ren J, Li W, Shu G, Yang J, Shen W, *et al*: CST1 inhibits ferroptosis and promotes gastric cancer metastasis by regulating GPX4 protein stability via OTUB1. Oncogene 42: 83-98, 2023.
10. Zhou P, Chen X, Shi K, Qu H and Xia J: The characteristics, tumorigenicities and therapeutics of cancer stem cells based on circRNAs. Pathol Res Pract 233: 153822, 2022.
11. Li H, Lan T, Liu H, Liu C, Dai J, Xu L, Cai Y, Hou G, Xie K, Liao M, *et al*: IL-6-induced cGGNBP2 encodes a protein to promote cell growth and metastasis in intrahepatic cholangiocarcinoma. Hepatology 75: 1402-1419, 2021.
12. Lu Q and Fang T: Circular RNA SMARCA5 correlates with favorable clinical tumor features and prognosis, and increases chemotherapy sensitivity in intrahepatic cholangiocarcinoma. J Clin Lab Anal 34: e23138, 2020.
13. Wang X, Xing L, Yang R, Chen H, Wang M, Jiang R, Zhang L and Chen J: The circACTN4 interacts with FUBP1 to promote tumorigenesis and progression of breast cancer by regulating the expression of proto-oncogene MYC. Mol Cancer 20: 91, 2021.
14. Chen Q, Wang H, Li Z, Li F, Liang L, Zou Y, Shen H, Li J, Xia Y, Cheng Z, *et al*: Circular RNA ACTN4 promotes intrahepatic cholangiocarcinoma progression by recruiting YBX1 to initiate FZD7 transcription. J Hepatol 76: 135-147, 2022.
15. Wang Q, Hao X, Xu G and Lv T: Downregulated KIF3B induced by miR-605-3p inhibits the progression of colon cancer via inactivating Wnt/β-Catenin. J Oncol 2021: 5046981, 2021.
16. Zeng Z, Zhou W, Duan L, Zhang J, Lu X, Jin L and Yu Y: Circular RNA circ-VANGL1 as a competing endogenous RNA contributes to bladder cancer progression by regulating miR-605-3p/VANGL1 pathway. J Cell Physiol 234: 3887-3896, 2019.
17. Liu N, Hu G, Wang H, Wang Y and Guo Z: LncRNA BLACAT1 regulates VASP expression via binding to miR-605-3p and promotes giloma development. J Cell Physiol 234: 22144-22152, 2019.

18. Hu YL, Feng Y, Chen YY, Liu JZ, Su Y, Li P, Huang H, Mao QS and Xue WJ: SNHG16/miR-605-3p/TRAF6/NF-κB feedback loop regulates hepatocellular carcinoma metastasis. J Cell Mol Med 24: 7637-7651, 2020.
19. Fei F, Li X, Xu L, Li D, Zhang Z, Guo X, Yang H, Chen Z and Xing J: CD147-CD98hc complex contributes to poor prognosis of non-small cell lung cancer patients through promoting cell proliferation via the PI3K/Akt signaling pathway. Ann Surg Oncol 21: 4359-4368, 2014.
20. Liu C, Li X, Li C, Zhang Z, Gao X, Jia Z, Chen H, Jia Q, Zhao X, Liu J, *et al*: SLC3A2 is a novel endoplasmic reticulum stress-related signaling protein that regulates the unfolded protein response and apoptosis. PLoS One 13: e0208993, 2018.
21. Palacín M and Kanai Y: The ancillary proteins of HATs: SLC3 family of amino acid transporters. Pflugers Arch 447: 490-494, 2004.
22. He J, Liu D, Liu M, Tang R and Zhang D: Characterizing the role of SLC3A2 in the molecular landscape and immune microenvironment across human tumors. Front Mol Biosci 9: 961410, 2022.
23. Koppula P, Zhuang L and Gan B: Cystine transporter SLC7A11/xCT in cancer: Ferroptosis, nutrient dependency, and cancer therapy. Protein Cell 12: 599-620, 2021.
24. Digomann D, Linge A and Dubrovska A: SLC3A2/CD98hc, autophagy and tumor radioresistance: A link confirmed. Autophagy 15: 1850-1851, 2019.
25. Ma L, Zhang X, Yu K, Xu X, Chen T, Shi Y, Wang Y, Qiu S, Guo S, Cui J, *et al*: Targeting SLC3A2 subunit of system X_C^- is essential for m^6A reader YTHDC2 to be an endogenous ferroptosis inducer in lung adenocarcinoma. Free Radic Biol Med 168: 25-43, 2021.
26. Wu F, Xiong G, Chen Z, Lei C, Liu Q and Bai Y: SLC3A2 inhibits ferroptosis in laryngeal carcinoma via mTOR pathway. Hereditas 159: 6, 2022.
27. Liu H, Deng Z, Yu B, Liu H, Yang Z, Zeng A and Fu M: Identification of SLC3A2 as a potential therapeutic target of osteoarthritis involved in ferroptosis by integrating bioinformatics, clinical factors and experiments. Cells 11: 3430, 2022.
28. Hu Z, Yin Y, Jiang J, Yan C, Wang Y, Wang D and Li L: Exosomal miR-142-3p secreted by hepatitis B virus (HBV)-hepatocellular carcinoma (HCC) cells promotes ferroptosis of M1-type macrophages through SLC3A2 and the mechanism of HCC progression. J Gastrointest Oncol 13: 754-767, 2022.
29. Qin X, Zhang J, Wang B, Xu G, Yang X, Zou Z and Yu C: Ferritinophagy is involved in the zinc oxide nanoparticles-induced ferroptosis of vascular endothelial cells. Autophagy 17: 4266-4285, 2021.
30. Shang A, Gu C, Wang W, Wang X, Sun J, Zeng B, Chen C, Chang W, Ping Y, Ji P, *et al*: Exosomal circPACRGL promotes progression of colorectal cancer via the miR-142-3p/miR-506-3p-TGF-β1 axis. Mol Cancer 19: 117, 2020.
31. Livak KJ and Schmittgen TD: Analysis of relative gene expression data using real-time quantitative PCR and the 2(-Delta Delta C(T)) method. Methods 25: 402-408, 2001.
32. Krenzien F, Nevermann N, Krombholz A, Benzing C, Haber P, Fehrenbach U, Lurje G, Pelzer U, Pratschke J, Schmelzle M and Schöning W: Treatment of intrahepatic cholangiocarcinoma-a multidisciplinary approach. Cancers (Basel) 14: 362, 2022.
33. Yang J, Qi M, Fei X, Wang X and Wang K: Hsa_circRNA_0088036 acts as a ceRNA to promote bladder cancer progression by sponging miR-140-3p. Cell Death Dis 13: 322, 2022.
34. Du J, Lan T, Liao H, Feng X, Chen X, Liao W, Hou G, Xu L, Feng Q, Xie K, *et al*: CircNFIB inhibits tumor growth and metastasis through suppressing MEK1/ERK signaling in intrahepatic cholangiocarcinoma. Mol Cancer 21: 18, 2022.
35. Jiang XM, Li ZL, Li JL, Xu Y, Leng KM, Cui YF and Sun DJ: A novel prognostic biomarker for cholangiocarcinoma: circRNA Cdr1as. Eur Rev Med Pharmacol Sci 22: 365-371, 2018.
36. Zhou D, Gao B, Yang Q, Kong Y and Wang W: Integrative analysis of ceRNA network reveals functional lncRNAs in intrahepatic cholangiocarcinoma. Biomed Res Int 2019: 2601271, 2019.
37. Kang Z, Guo L, Zhu Z and Qu R: Identification of prognostic factors for intrahepatic cholangiocarcinoma using long non-coding RNAs-associated ceRNA network. Cancer Cell Int 20: 315, 2020.
38. Xu YP, Dong ZN, Wang SW, Zheng YM, Zhang C, Zhou YQ, Zhao YJ, Zhao Y, Wang F, Peng R, *et al*: circHMGCS1-016 reshapes immune environment by sponging miR-1236-3p to regulate CD73 and GAL-8 expression in intrahepatic cholangiocarcinoma. J Exp Clin Cancer Res 40: 290, 2021.
39. Tang J, Wang R, Tang R, Gu P, Han J and Huang W: CircRTN4IP1 regulates the malignant progression of intrahepatic cholangiocarcinoma by sponging miR-541-5p to induce HIF1A production. Pathol Res Pract 230: 153732, 2022.
40. Cano-Crespo S, Chillarón J, Junza A, Fernández-Miranda G, García J, Polte C, R de la Ballina L, Ignatova Z, Yanes Ó, Zorzano A, *et al*: CD98hc (SLC3A2) sustains amino acid and nucleotide availability for cell cycle progression. Sci Rep 9: 14065, 2019.
41. Furuya M, Horiguchi J, Nakajima H, Kanai Y and Oyama T: Correlation of L-type amino acid transporter 1 and CD98 expression with triple negative breast cancer prognosis. Cancer Sci 103: 382-389, 2012.
42. Zhu B, Cheng D, Hou L, Zhou S, Ying T and Yang Q: SLC3A2 is upregulated in human osteosarcoma and promotes tumor growth through the PI3K/Akt signaling pathway. Oncol Rep 37: 2575-2582, 2017.
43. Li W, Dong X, He C, Tan G, Li Z, Zhai B, Feng J, Jiang X, Liu C, Jiang H and Sun X: LncRNA SNHG1 contributes to sorafenib resistance by activating the Akt pathway and is positively regulated by miR-21 in hepatocellular carcinoma cells. J Exp Clin Cancer Res 38: 183, 2019.
44. Janpipatkul K, Suksen K, Borwornpinyo S, Jearawiriyapaisarn N, Hongeng S, Piyachaturawat P and Chairoungdua A: Downregulation of LAT1 expression suppresses cholangiocarcinoma cell invasion and migration. Cell Signal 26: 1668-1679, 2014.